Interference Analysis for Highly Directional 60-GHz Mesh Networks: The Case for Rethinking Medium Access Control

Sumit Singh, *Member, IEEE*, Raghuraman Mudumbai, *Member, IEEE*, and Upamanyu Madhow, *Fellow, IEEE*

***Abstract*—We investigate spatial interference statistics for multigigabit outdoor mesh networks operating in the unlicensed 60-GHz "millimeter (mm) wave" band. The links in such networks are highly directional: Because of the small carrier wavelength (an order of magnitude smaller than those for existing cellular and wireless local area networks), narrow beams are essential for overcoming higher path loss and can be implemented using compact electronically steerable antenna arrays. Directionality drastically reduces interference, but it also leads to "deafness," making implicit coordination using carrier sense infeasible. In this paper, we make a quantitative case for rethinking medium access control (MAC) design in such settings. Unlike existing MAC protocols for omnidirectional networks, where the focus is on interference management, we contend that MAC design for 60-GHz mesh networks can essentially ignore interference and must focus instead on the challenge of scheduling half-duplex transmissions with deaf neighbors. Our main contribution is an analytical framework for estimating the collision probability in such networks as a function of the antenna patterns and the density of simultaneously transmitting nodes. The numerical results from our interference analysis show that highly directional links can indeed be modeled as *pseudowired*, in that the collision probability is small even with a significant density of transmitters. Furthermore, simulation of a rudimentary directional slotted Aloha protocol shows that packet losses due to failed coordination are an order of magnitude higher than those due to collisions, confirming our analytical results and highlighting the need for more sophisticated coordination mechanisms.**

***Index Terms*—60-GHz networks, interference analysis, medium access control (MAC), millimeter (mm) wave networks, wireless mesh networks.**

Manuscript received June 07, 2010; revised November 24, 2010; accepted February 09, 2011; approved by IEEE/ACM TRANSACTIONS ON NETWORKING Editor K. Papagiannaki. Date of publication March 17, 2011; date of current version October 14, 2011. This work was supported in part by the National Science Foundation under Grant CNS-0832154 and by the Institute for Collaborative Biotechnologies under Contract W911NF-09-D-0001 from the U.S. Army Research Office.

S. Singh was with the Department of Electrical and Computer Engineering, University of California, Santa Barbara, CA 93106 USA. He is now with the Moseley Wireless Solutions Group, Santa Barbara, CA 93117 USA (e-mail: ssingh@moseleysb.com).

R. Mudumbai is with the Department of Electrical and Computer Engineering, The University of Iowa, Iowa City, IA 52242 USA (e-mail: rmudumbai@engineering.uiowa.edu).

U. Madhow is with the Department of Electrical and Computer Engineering, University of California, Santa Barbara, CA 93106 USA (e-mail: madhow@ece.ucsb.edu).

Color versions of one or more of the figures in this paper are available online at http://ieeexplore.ieee.org.

Digital Object Identifier 10.1109/TNET.2011.2122343

I. INTRODUCTION

THE SEVERAL gigahertz of unlicensed spectrum available worldwide in the 60-GHz "millimeter (mm) wave" band, coupled with the recent progress in low-cost mm-wave radio-frequency integrated circuit (RFIC) design, indicates that the mass market deployment of multigigabit wireless networks is on the cusp of feasibility. There is significant industry interest in indoor applications of this technology to wireless personal area networks [1]–[3], wireless local area networks [4], and wireless uncompressed HDTV [5]. However, use of the 60-GHz band is also very attractive for *outdoor* mesh networks with relatively short link ranges of 100–200 m: Oxygen absorption in the 60-GHz band produces propagation losses of 10–16 dB/km, so it only adds about 3 dB to the link budget for a 200-m link. Such multigigabit outdoor mesh networks provide an easily deployable broadband infrastructure that can have a multitude of applications, including wireless backhaul for picocellular networks and as an alternative to fiber to the home. Our goal in this paper, however, is to point out that in order to realize the potential for such networks, it is necessary to rethink the design of network protocols, accounting for the unique physical characteristics of mm-wave links. In particular, we observe that links in such networks must be highly directional and provide a framework for analyzing the spatial interference statistics in order to obtain quantitative guidelines for medium access control (MAC) design.

The fundamental distinguishing feature of the 60-GHz band relative to, say, the 2.4-GHz WiFi band, is the order of magnitude difference in wavelength. For omnidirectional communication, free-space propagation loss scales as λ^2, where $\lambda = c/f_c$ is the carrier wavelength, with c denoting the speed of light and f_c the carrier wavelength. The wavelength at 60 GHz is 5 mm, while the wavelength at 2.4 GHz (WiFi band) is 12.5 cm, so the propagation loss for omnidirectional transmission and reception is 625 times, or 28 decibels (dB), worse at 60 GHz than at 2.4 GHz. On the other hand, for a given antenna aperture, directivity scales as $\frac{1}{\lambda^2}$. Thus, fixing the antenna aperture at each end, we gain by a factor of $\frac{1}{\lambda^4}$, making the overall propagation coefficient scale as $\frac{1}{\lambda^2}$; this corresponds to a net *gain* of 28 dB in going from 2.4 to 60 GHz. Thus, given the difficulty of producing large amounts of radio frequency (RF) power at mm-wave frequencies using low-cost silicon implementations, employing highly directive antennas at both transmitter and receiver is *essential* for the range/rate combinations we wish to achieve. Fortunately, the small carrier wavelength also allows

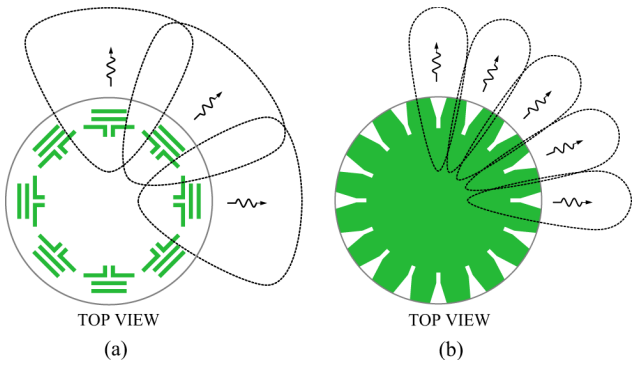

Fig. 1. Steerable arrays with high directivity are realizable with compact form factors. Each element in the array can have significant directivity (e.g., up to 20 dBi), and combining several elements with overlapping fields of view can achieve directivities on the order of 25–30 dBi. (a) Yagi–Uda antenna array. (b) Open-slot antenna array.

for the realization of compact, electronically steerable antenna arrays (with elements realized as patterns of metal on circuit board), as demonstrated in [6] and [7]. While hardware is not the focus of this paper, we note that it is possible to design nodes that provide steerable narrow beams, while providing a 360° field of view; see Fig. 1 for a concept design. Such *omnicoverage yet highly directional* nodes are the analog of omnidirectional nodes at lower carrier frequencies and enable plug-and-play deployment since they can steer highly directional beams to neighbors in any direction.

Wireless networks at lower carrier frequencies typically employ omnidirectional (or mildly directional) links, so interference is the main performance bottleneck. Thus, conventional MAC design for such networks focuses on mechanisms for interference management. In this paper, we make a quantitative argument that a drastic rethinking of this approach is needed for the design of MAC protocols for 60-GHz mesh networks. The high directivity of 60-GHz links implies that the interference among simultaneously active links can be expected to be significantly smaller than for omnidirectional links. It also leads to deafness: We can no longer count on nodes being able to monitor transmissions destined for other nodes, so the use of coordination mechanisms such as carrier sense or broadcast control messages becomes infeasible. We argue, therefore, that MAC design for highly directional 60-GHz networks can ignore interference up to the first order (e.g., by being reactive rather than proactive about interference management) and should focus attention instead on the problem of transmitter–receiver coordination in the face of deafness. While our focus in this paper is to quantitatively justify these new design guidelines rather than to present a candidate MAC protocol, we note that preliminary results for a distributed MAC protocol designed based on these guidelines are promising [8].

The contributions of this paper can be summarized as follows.

- We analyze the statistics of the spatial interference due to multiple simultaneous and uncoordinated transmissions, with transmitters distributed uniformly on the plane and link orientations chosen randomly. The collision probability at a designated receiver is computed as a function of the node density and antenna pattern, and the analysis accounts for square law line-of-sight propagation loss as well as the exponential loss due to oxygen absorption. We consider both a "protocol model" (where a collision occurs if some interferer exceeds a threshold) and a "physical model" (in which the sum interference exceeds a threshold), where the terminology is borrowed from the work of Gupta and Kumar [9].
- Our numerical results show that, for the antenna directivities that we envision, the collision probability is small even without any coordination among transmitters. This motivates a *pseudowired* abstraction to serve as a first-order approximation of mm-wave wireless links for the purpose of MAC design. Under this abstraction, transmissions on different links do not interfere with each other. However, unlike a truly wired node, mm-wave network nodes have a half-duplex constraint, i.e., they can either send or receive at a given time, but not both. This allows MAC designers to concentrate on developing lightweight protocols to schedule transmissions in a "deaf" network subject to half-duplex constraints.
- We verify that transmitter–receiver coordination is indeed the bottleneck by simulating a directional slotted Aloha protocol for 60-GHz mesh networks with random topologies. The simulation results show that packet losses due to failed coordination are an order of magnitude higher than those due to collision.

The results in this paper build on the preliminary results presented in our conference publication [10]. While our conference publication employed Monte Carlo simulations for estimating collision probabilities for the physical model, a major new contribution in this paper is that we provide new analytical approaches that yield good approximations as well as tight upper bounds. We also provide a more extensive set of numerical results, including simulation results for a directional slotted Aloha protocol illustrating the need for internode coordination. Finally, we provide a detailed description of the directive antenna patterns used in our numerical results.

The rest of this paper is organized as follows. Section II outlines related work. In Section III, we describe our mm-wave network model. In Section IV, we analyze the statistics of interference with highly directional antennas, assuming a randomly deployed network with uncoordinated transmissions. Section V presents simulation results for a directional slotted Aloha protocol. Finally, conclusions and future work are discussed in Section VI.

II. Related Work

There is a significant prior (and growing) literature on 60-GHz *indoor* personal area network design, propagation modeling, and link measurements; see [11]–[13] and the references therein. While MAC design ideas developed for outdoor networks may be applicable in this domain as well, additional considerations such as blockage and the coexistence of a number of different applications may also become important in the indoor setting.

There is extensive literature on directional networking for cellular, broadband, and WiFi-based multihop wireless networks operating over lower frequency bands [14]–[19]. Most of

the directional networking proposals for multihop wireless networks employ a combination of directional and omnidirectional communication for protocol operation and data transfer. These approaches exploit the broadcast nature of omnidirectional transmissions for critical control message propagation, thereby avoiding some of the coordination issues that arise or are exacerbated on being fully directional (such as neighbor discovery and deafness). This dual-mode operation is not appropriate for the mm-wave mesh networks, where very high directionality is required simply to achieve a reliable high data rate link. There are a few recent proposals on fully directional protocols for multihop wireless networks [20]–[22]. However, the directivity achievable at the lower frequency bands considered by these papers is much smaller, so the focus of MAC design is still on interference management, unlike the pseudowired abstraction that follows from the interference analysis in our paper.

There is also a significant body of previous work on modeling the statistics of interference in wireless networks. Gupta and Kumar, in their influential contribution on wireless capacity [9] introduced two different models for interference, i.e., the "protocol model" and "physical model." The protocol model corresponds to the collision model that has historically been very influential in MAC design for packet-radio networks [23], while the physical model has been commonly used to model cochannel interference [24] in cellular networks. For the latter application, a Gaussian approximation for the aggregate interference [24], [25], motivated by the Central Limit Theorem, has been proposed. However, the limits of the Gaussian model especially for channels with small numbers of users and highly varying channel fading gains has been widely recognized [26]. The validity of the simplifying assumptions underlying the different interference models was explored in [27], which also provides a survey of the models used in MAC design. The authors in [27] show that results from simple interference models similar to the protocol model can deviate significantly from a more accurate model based on the SINR with sum interference calculation (i.e., the physical model).

We have recently learned that an analytical approach similar to ours has been employed in the information theory literature for characterizing outage probabilities in omnidirectional networks; see [28] and the references therein. The approach is conceptually similar in that it assumes transmissions are uncoordinated and distributed according to a Poisson process on a plane and that the interference is decomposed into "near" and "far" interferers. Of course, the details of the analysis for our 60-GHz setting are quite different because of the highly directional nature of the transmissions and the exponential oxygen absorption loss.

To the best of our knowledge, except for the preliminary results presented in the conference paper [10] that we expand upon here, this paper is the first to characterize spatial interference in mm-wave mesh networks and to quantitatively justify a pseudowired abstraction for MAC design. We have followed up on these MAC design guidelines in another conference paper [8], where we present a MAC protocol that employs memory and learning to address deafness, while exploiting the reduction of interference between simultaneous transmissions to take a reactive rather than a proactive approach to interference management.

III. Network Model

We consider a Poisson distribution of nodes over a large area A with a density ρ_s. If we now randomly select a subset of nodes as transmitters, the distribution of transmitters on the area of interest is also Poisson, with density $\rho = \rho_s p_{\mathrm{t}}$ where p_{t} is the probability that the selected node is transmitting. Therefore, the number of transmit nodes N_{T} over a deployment area A is a Poisson random variable with mean ρA.

We assume that each node can communicate with at most one other node at any given time slot. In other words, we do not rely on advanced physical-layer capabilities such as spatial multiplexing or multiuser detection. If multiple neighbors are transmitting to the same receiver, at most one of them can be successfully decoded by the receiver. All other transmissions in the network act as interference for the receiver. The amount of interference depends on the location of the interferer relative to the receiver and the radiation patterns of the antennas at the receiver and the interferer. We assume that a transmission is successfully decoded by the receiver if the total signal-to-interference-plus-noise ratio (SINR) is above a given threshold, say β. Otherwise, a *collision* occurs, and the transmission is lost. For simplicity of analysis, we ignore thermal noise and only consider interference while calculating SINR. Similar network models that draw upon stochastic geometry (e.g., randomizing transmitter locations over the network deployment area) have been used for transmission capacity and interference analysis for low-frequency wireless networks [28].

A. Nominal Link

The standard Friis transmission equation for mm waves gives the received power as a function of range r as

$$P_{\mathrm{Rx}}(r) = P_{\mathrm{Tx}} G_{\mathrm{Rx}} G_{\mathrm{Tx}} \left(\frac{\lambda}{4\pi r}\right)^2 e^{-\alpha r} \tag{1}$$

where P_{Tx} is the transmitted power; G_{Rx}, G_{Tx} are the gains of the receive and transmit antennas, respectively; λ is the wavelength; and α is the attenuation factor due to absorption in the medium. For an mm-wave link at 60 GHz, $\lambda = 5$ mm. Parameter α captures the oxygen absorption loss that can be as high as 16 dB/km [29] (for oxygen absorption of 16 dB/km, $\alpha = 0.0016 * \log_e(10) = 0.0037$/m). Since lower absorption rate leads to *more* interference, we use a conservative oxygen absorption value of 10 dB/km ($\alpha = 0.0023/\mathrm{m}$) in our numerical results.

We assume that each transmitter–receiver pair uses beamsteering to maximize the signal power on the respective link without regard to the interference. Thus, the received power at a reference link distance of R_0 (e.g., $R_0 = 100$ and 200 m in our numerical results) is denoted by $P_0 = P_{\mathrm{Rx}}(R_0)$, with $G_{\mathrm{Tx}} = G_{\mathrm{Rx}} = G_{\max}$, where $G_{\max}$ denotes the maximum antenna gain.

Consider the link budget for a 2-Gb/s line-of-sight (LoS) link, assuming quadrature phase shift keying (QPSK) signaling, a desired SINR of 14 dB [which allows for uncoded QPSK modu-

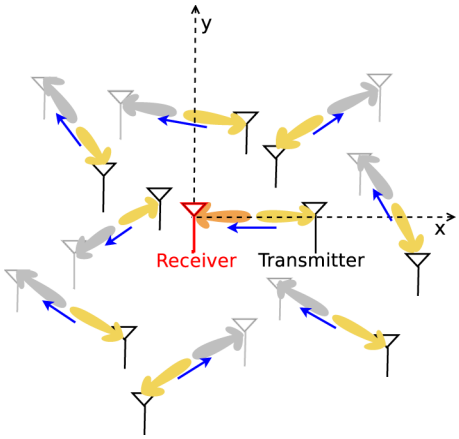

Fig. 2. Network model for interference analysis.

lation at a bit error rate (BER) of 10^{-9}], oxygen absorption loss of 10 dB/km, and 10 mW transmit power. For a desired link range of $R_0 = 100$ m, we need antenna gains of about 24 dBi at both the transmitter and receiver in order to provide a 10-dB link margin. For link range $R_0 = 200$ m, the required antenna gains at the transmitter and the receiver increase to 27 dBi. These link parameters are used as a baseline for the rest of the paper.

Our setting for interference analysis is as follows. Consider the transmitter–receiver pair shown in Fig. 2. Without loss of generality, assume that the receiver is located at the origin and is communicating with the transmitter located along the x-axis at a distance equal to the reference link distance R_0 while undergoing interference from other concurrent transmissions. The other $N_{\mathrm{T}} - 1$ interfering transmitters are transmitting to corresponding receivers located at randomly chosen orientations.

B. Antenna Pattern

Directional antennas are characterized by their pattern functions that measure the power gain $G(\theta, \phi)$ over the spherical elevation and azimuthal angle coordinates θ and ϕ. The directivity D of an antenna (which equals the antenna gain for a lossless antenna) is the ratio of the maximum power density and the average power density over a sphere. It is given by

$$D = \frac{4\pi}{\Omega} \tag{2}$$

where $\Omega = \int_{\theta=0}^{\pi} \int_{\phi=-\pi}^{\pi} G_n(\theta, \phi) \sin\theta \, d\theta \, d\phi$ is the *beam area* or *beam solid angle* of the antenna in steradians and $G_n(\theta, \phi)$ is the normalized power pattern of the antenna.

Without loss of generality, we assume that all nodes are on the same horizontal plane. We do not consider variation in beam pattern over the elevation angle θ and work with the normalized 2-D pattern

$$g(\phi) \triangleq \frac{G(0, \phi)}{G_{\max}} \qquad \text{where } G_{\max} = \max_{\phi} G(0, \phi). \tag{3}$$

We define the azimuthal *beam angle* of the antenna as

$$\Delta\phi = \int_{\phi=-\pi}^{\pi} g(\phi) d\phi. \tag{4}$$

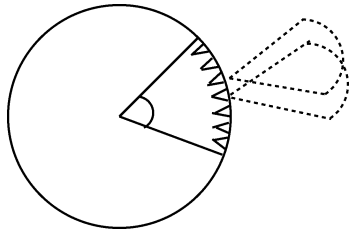

Fig. 3. Approximating a circular array of slot antennas as a uniform linear array of flat-top elements.

One idealization that proves to be very useful for our interference analysis is that of a sectorized "flat-top" directional antenna, which has unit gain within its beam angle $\Delta\phi_{\mathrm{ft}}$ and zero gain outside. More precisely

$$g(\phi) = \begin{cases} 1, & |\phi| \le \frac{\Delta\phi_{\mathrm{ft}}}{2} \\ 0, & \text{otherwise.} \end{cases} \tag{5}$$

In 3-D, the flat-top antenna beam is assumed to be symmetric about the beam-axis, so the azimuthal beam angle and the elevation beam angle are equal.

While the flat-top antenna is a useful idealization, practical directional antenna gains have a more complex dependence on the azimuth angle. For instance, sidelobes in the gain function could cause significant interference even in directions far from the antenna boresight. While exact computation of the gain functions of practical mm-wave antenna arrays can be messy (because array elements are directional themselves), we can obtain useful models with some simplifying assumptions. In a circular array of directional antenna elements, only a subset of the array elements with significantly overlapping main lobes contribute to the antenna gain in any specific direction. The number of elements in this subset can still be quite large. For instance, if the diameter of the overall array is 10 cm and the interelement spacing is a half-wavelength and each element has an azimuthal beamwidth of, say, 120°, we can have on the order of 20–30 elements with overlapping beams. If we assume that the beams of these elements are approximately flat within the main lobe and neglect the curvature of their placement, we can approximate this subarray as a uniform linear array, each of whose elements has a flat-top response. In particular, we obtain the following normalized power gain pattern for an N-element linear array in which each individual flat-top element has beam angle (or sector size) $\Delta\phi_{\mathrm{ft}}$ and is placed $\frac{\lambda}{2}$ apart:

$$g(\phi) = \begin{cases} \frac{1}{N^2} \frac{\sin^2\left(\frac{N}{2}\pi \sin\phi\right)}{\sin^2\left(\frac{1}{2}\pi \sin\phi\right)}, & |\phi| \le \frac{\Delta\phi_{\mathrm{ft}}}{2} \\ 0, & \text{otherwise.} \end{cases} \tag{6}$$

Fig. 3 illustrates how to approximate a circular array with a linear array of flat-top elements. Fig. 4 shows the gain patterns for a narrow-beam flat-top antenna with beam angle 14.4° and a 12-element linear array of flat-top elements, each of sector size 20°. The antenna directivity in both cases is 24 dBi. The corresponding directivity computations are described in the Appendix.

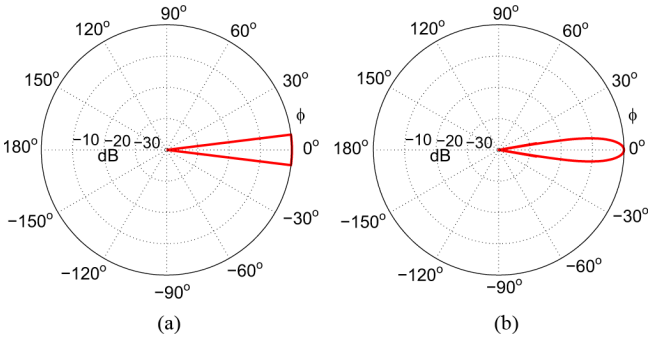

Fig. 4. Gain pattern for (a) a flat-top antenna and (b) a linear array of flat-top elements.

IV. Interference Analysis

We now analyze the probability of packet loss due to interference. We consider two different models of interference. In the protocol model of interference, a packet loss occurs if and only if there is some interfering node whose signal at the receiver exceeds a given threshold. Nodes located far away from the receiver cannot cause interference in this model. In the physical model, a packet loss occurs when the total interference from all nodes exceeds a given threshold. Under this model, it is possible for the sum interference from a number of nodes to cause packet failure, even if the interfering signal from each of them may be individually too weak to cause a collision. The two models can be summarized as follows:

$$\Pr(\text{collision}) \triangleq \begin{cases} \Pr\left(\max\limits_{1\le k\le N_{\mathrm{T}}-1} P_k \ge \frac{1}{\beta}P_0\right), & \text{(protocol model)} \\ \Pr\left(\sum\limits_{k=1}^{N_{\mathrm{T}}-1} P_k \ge \frac{1}{\beta}P_0\right), & \text{(physical model)} \end{cases}$$

where P_k is the power at the receiver of the signal from the kth interferer. Since $\sum_{k=1}^{N_{\mathrm{T}}-1} P_k \ge \max_{1\le k\le N_{\mathrm{T}}-1} P_k$, it follows that $\Pr(\text{collision})$ for the physical model is lower-bounded by the corresponding value for the protocol model.

We first derive an expression for the collision probability for a "typical" node in the interior of a large network under the protocol model for the flat-top antenna. The flat-top antenna interference analysis under the protocol model, while being simple and intuitive, offers valuable insight into the key trends obtained from the more rigorous models presented later in this section. We then extend the analysis to general directional antenna models that account for sidelobes. We next estimate $\Pr(\text{collision})$ with the physical model.

Our analytical approach for the protocol model is inspired by the analysis of localization error in [30]. We note that our analysis applies to the network as a whole. The collision probability for a typical node in the interior of a large network provides a pessimistic estimate of the average collision rate over the network since it ignores edge effects (i.e., nodes on the edge of the network would experience less interference than those in the interior).

A. Protocol Model With Ideal Flat-Top Antennas

For the ideal flat-top antenna, only interferers located within the boresight of the receiver can cause a collision (see Fig. 5).

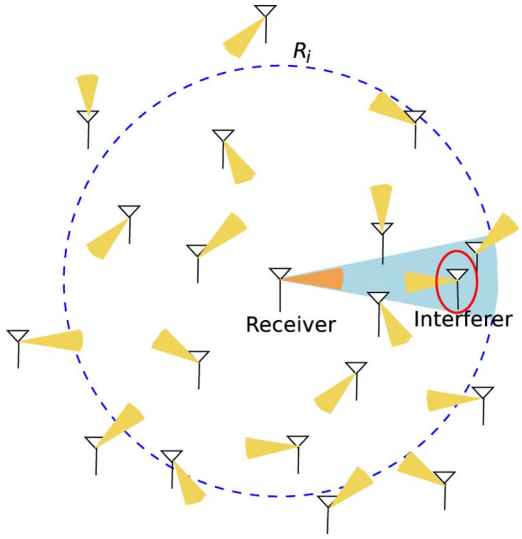

Fig. 5. Protocol model with flat-top antennas.

Furthermore, a transmitting node within this sector causes interference only if the receiver is within its boresight, which has probability $q = \frac{\Delta\phi}{2\pi}$, since the potentially interfering transmitter is sending to a randomly chosen receiver.

Let R_i be the *interference range*, i.e., the maximum distance an interferer can be from the receiver and still cause a collision. Using (1), the signal and interference powers are evaluated as

$$P_{\mathrm{Rx}}(R_0) \equiv P_0 = P_{\mathrm{Tx}} G_{\max}^2 \left(\frac{\lambda}{4\pi R_0}\right)^2 e^{-\alpha R_0} \tag{7}$$

$$P_{\mathrm{interf}}(R_i) = P_{\mathrm{Tx}} G_{\max}^2 \left(\frac{\lambda}{4\pi R_i}\right)^2 e^{-\alpha R_i} = P_0 \frac{R_0^2}{R_i^2} e^{-\alpha(R_i - R_0)} \tag{8}$$

where we used $G_{\mathrm{Tx}} = G_{\mathrm{Rx}} = G_{\max}$ for the antenna gains assuming that the interferer and the receiver are within each other's boresights. We set $P_{\mathrm{Rx}}(R_0) = P_0$: When the transmitter and receiver are steered toward each other, this is the signal power designed for at the reference distance R_0. Using the collision condition for obtaining the interference range R_i, $P_{\mathrm{interf}}(R_i) = \frac{1}{\beta}P_0$, we can rewrite (8) as

$$\frac{R_i^2}{R_0^2} e^{\alpha(R_i - R_0)} = \beta \tag{9}$$

which determines R_i as a function of the SINR threshold β. Fig. 6 plots R_i as a function of β for a mm-wave mesh link of range $R_0 = 100$ m, with $\alpha = 0.0023$/m.

The number of potentially interfering transmitters is therefore a Poisson random variable with mean $\mu_i = \rho A_i$, where $A_i = \frac{1}{2}\Delta\phi R_i^2$. The probability of any of these actually causing a collision is $q = \frac{\Delta\phi}{2\pi}$, so the number of interferers N_i causing a collision is also a Poisson random variable, with mean $q\mu_i$. The probability of a collision is therefore given by

$$\Pr(\text{collision}) \equiv \Pr(N_i > 0) = 1 - e^{-q\mu_i} = 1 - e^{-\frac{(\Delta\phi)^2}{4\pi}\rho R_i^2} = 1 - e^{-\rho A_{\mathrm{c}}} \tag{10}$$

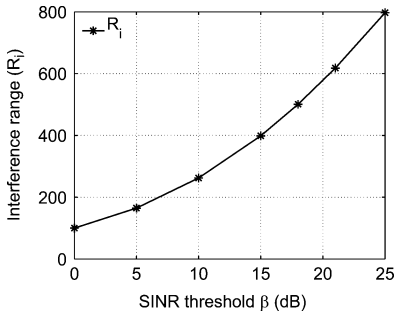

Fig. 6. Interference range R_i for $R_0 = 100$ m, from (9).

where

$$A_{\rm c} = \frac{(\Delta\phi)^2}{4\pi}\beta R_0^2 e^{-\alpha(R_i - R_0)}. \tag{11}$$

From (10), $A_{\rm c} = q^2\pi R_i^2$ can be interpreted as the "expected interference area" around the receiver, equal to the region spanned by the interference range (πR_i^2) scaled down by q^2, the probability that the receiver and the interferer are within each other's boresight.

For a beam angle of $\Delta\phi = \frac{\pi}{18}$ radians (10°), $\beta = 15$ dB and $\rho R_0^2 = 1$ corresponding to roughly $\pi\rho R_0^2 \approx 3$ potential interferers within communication range $R_0 = 100$ m and 50 potential interferers within the interference range $R_i = 400$ m of each receiver, (10) gives an estimate of $\Pr(\text{collision}) \approx 3.8\%$. The substantially low collision probability in this example suggests that acceptable MAC performance may be possible with minimal coordination for interference management.

B. Protocol Model With General Directional Antennas

We now generalize (10) for a general directional antenna pattern. We first compute the probability of collision due to a single interferer randomly located at a distance R and angle ϕ_1 relative to the receiver as shown in Fig. 7. The angle ϕ_2 represents the direction of the interferer's beam relative to the receiver. We model ϕ_1, ϕ_2 as independent and uniformly distributed over $(-\pi, \pi]$, given the random orientation of the interfering transmitter and its beam relative to the desired receiver. Signal power is still given by (7), and the interference power is

$$P_{\rm interf}(R) = P_{\rm Tx} G_{\rm max}^2 g(\phi_1) g(\phi_2) \left(\frac{\lambda}{4\pi R}\right)^2 e^{-\alpha R} \tag{12}$$

where we used $G_{\rm Rx} = G_{\rm max} g(\phi_1)$ and $G_{\rm Tx} = G_{\rm max} g(\phi_2)$. Using (7), we can rewrite (12) as

$$P_{\rm interf}(R) = P_0 g(\phi_1) g(\phi_2) \left(\frac{R_0}{R}\right)^2 e^{-\alpha(R - R_0)}. \tag{13}$$

We define $X = \frac{P_{\rm interf}(R)}{P_0}$, the normalized interference power due to a transmitter randomly oriented and randomly placed at a distance R from the receiver. Therefore

$$X(\phi_1, \phi_2, R) = g(\phi_1) g(\phi_2) \left(\frac{R_0}{R}\right)^2 e^{-\alpha(R - R_0)}. \tag{14}$$

From the uniform spatial distribution of nodes, the conditional cumulative distribution function (cdf) $F_R(r)$ of the random variable R representing the interferer distance (i.e., the probability that an interfering node is within a distance r of the desired receiver, given that it is within area A) is $F_R(r) = \frac{\pi r^2}{A}$, which yields the conditional probability density function (pdf) $f_R(r)$ as, $f_R(r) = \frac{d}{dr}(F_R(r)) = \frac{2\pi r}{A}$. The distribution of X is determined by random variables R, ϕ_1, and ϕ_2 that are mutually independent. Define X_i as the normalized interference caused by an interferer i: X_i are independent and identically distributed (i.i.d.) random variables with the preceding probability distribution.

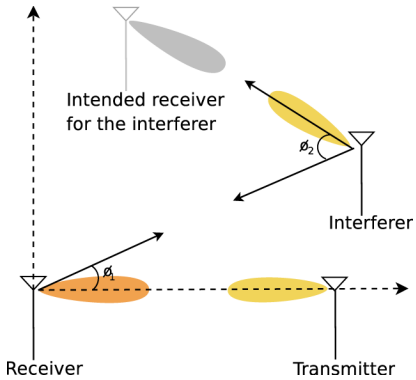

Fig. 7. Geometry of interference with directional antennas.

Therefore, the probability $p_{\rm c}$ that an interferer would cause a collision is

$$\begin{aligned} p_{\rm c} &= \Pr\left(X \geq \frac{1}{\beta}\right) \\ &= \iint_{(r,\phi_1)\in A} \int_{\phi_2=-\pi}^{\pi} \mathbf{1}\left(g(\phi_1)g(\phi_2)\frac{R_0^2}{r^2}e^{-\alpha(r-R_0)} \geq \frac{1}{\beta}\right) \\ &\quad \times \frac{2\pi r}{A}\frac{1}{4\pi^2} dr\, d\phi_1\, d\phi_2 \\ &= \frac{A_{\rm c}}{A} \end{aligned} \tag{15}$$

where $\mathbf{1}(\cdot)$ is the indicator function that takes the value 1 when its argument is true, and 0 otherwise, and

$$\begin{aligned} A_{\rm c} \doteq & \iint_{(r,\phi_1)\in A} \int_{\phi_2=-\pi}^{\pi} \mathbf{1}\left(g(\phi_1)g(\phi_2)\frac{R_0^2}{r^2}e^{-\alpha(r-R_0)} \geq \frac{1}{\beta}\right) \\ & \times \frac{1}{2\pi} r dr\, d\phi_1\, d\phi_2. \end{aligned} \tag{16}$$

We now consider $N_{\rm T} - 1$ interferers placed randomly in the area A. Each interferer has a collision probability $p_{\rm c}$ with the receiver given by (15). A collision occurs if at least one of these interferers causes a collision. The probability of collision is given by

$$\begin{aligned} \Pr(\text{collision}) &= 1 - (1 - p_{\rm c})^{N_{\rm T}-1} \qquad (17) \\ &= 1 - \lim_{A \to \infty} \left(1 - \frac{A_{\rm c}}{A}\right)^{\rho A} \\ &= 1 - e^{-\rho A_{\rm c}}. \qquad (18) \end{aligned}$$

Note that (18) has an identical form to (10) and that the collision probability depends on the antenna pattern only through

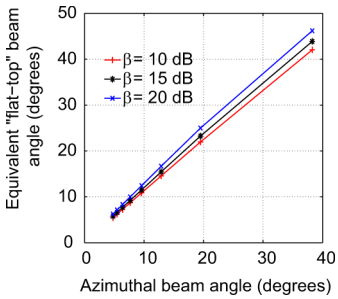

Fig. 8. Equivalent flat-top beam angle (link range = 100 m).

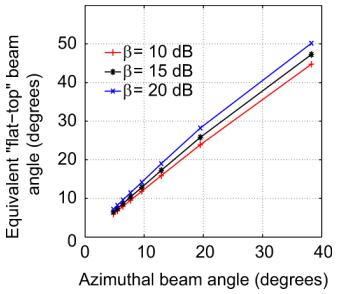

Fig. 9. Equivalent flat-top beam angle (link range = 200 m).

A_c. Thus, for the protocol model, we can restrict attention to an *equivalent flat-top model* in the azimuthal plane where the general directional antenna of each node is replaced by a flat-top antenna whose beam angle $\Delta\phi_{\text{eq}}$ can be calculated by evaluating A_c using (16) and plugging into (11) to obtain $\Delta\phi_{\text{eq}} \triangleq \sqrt{\frac{4\pi A_c}{\beta R_0^2}} e^{\frac{\alpha}{2}(R_i - R_0)}$. For instance, a six-element linear array of flat-top antennas of sector size 120° and half-wavelength spacing has an *equivalent flat-top beam angle* of about 23° for $\alpha = 10$ dB/km, $R_0 = 100$ m, and $\beta = 15$ dB. The algebraic azimuthal beam angle for the same linear array, given by (4), is about 20°. Figs. 8 and 9 show the equivalent flat-top beam angles for linear arrays of different numbers of flat-top elements of sector size 120° and half-wavelength spacing, for communication ranges of 100 and 200 m. As seen from the figure, the equivalent flat-top beam angle is numerically close to the algebraic beam angle given by (4) and does not vary much with the SINR threshold β.

C. Physical Model

In the protocol model, only nodes located within a bounded distance from the receiver are capable of causing a collision. On the other hand, under the physical model, interfering signals from a large number of faraway transmitters could, in principle, sum up at the receiver to cause packet reception failure. It turns out that the statistical properties of interference random variable $X(\phi_1, \phi_2, R)$ [defined in (14)] are such that the tail probabilities do not die fast enough, leading to a probability distribution skewed away from the small mean value in the positive direction, with a high variance. We find that the traditional upper-bound techniques such as Chernoff and Markov-type bounds do not work well when applied directly to characterize the sum interference over a large area. Furthermore, applying the Central Limit Theorem (CLT) on the sum interference does not yield

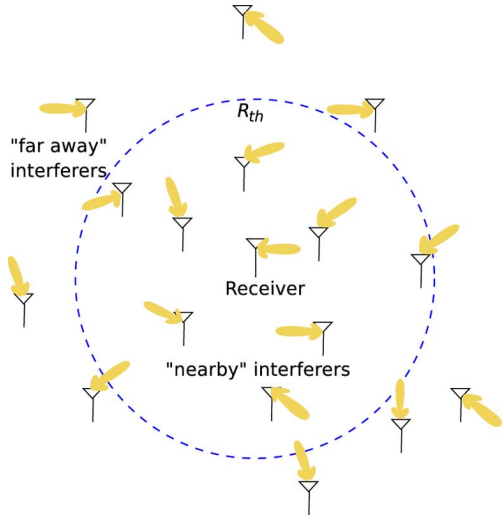

Fig. 10. Interference with the physical model: a hybrid approach.

reasonable $\Pr(\text{collision})$ estimates for typical node densities of interest.

While the protocol model collision probability serves as a lower bound for the collision probability under the physical model, we separately consider the effects of "faraway" and "nearby" interferers (say, within a circular region $C_{R_{\text{th}}}$ of radius R_{th} centered at the receiver) in order to obtain an approximation and an upper bound for the collision probability. We bound the effect of faraway interferers by applying the Markov inequality. We employ techniques similar to the protocol model to capture the effect of dominant nearby interferers (i.e., that can individually cause a packet loss at the receiver), while the aggregate interference from the nondominant nearby interferers is characterized via the CLT to obtain an approximation and the Chernoff bound to compute an upper bound for the collision probability. We find that the CLT-based approximation provides an accurate estimate for the collision probability over a wide range of parameter choices even when the bounds are not necessarily very tight. Fig. 10 illustrates the setting.

Let r_i be the distance of the ith interferer from the receiver. We write the total normalized interference power as the sum of two contributions X_{near} and X_{far}, defined as

$$X_{\text{near}} \triangleq \sum_{\{i: r_i \le R_{\text{th}}\}} X_i \quad X_{\text{far}} \triangleq \sum_{\{i: r_i > R_{\text{th}}\}} X_i \qquad (19)$$

where R_{th} is a suitable large distance. Then, we have

$$\begin{aligned}\Pr(\text{collision}) &= \Pr\left(X_{\text{near}} + X_{\text{far}} \ge \frac{1}{\beta}\right) \\ &\le \Pr\left(X_{\text{far}} \ge \Delta X\right) + \Pr\left(X_{\text{near}} \ge X_{\text{T}}\right) \qquad (20)\end{aligned}$$

where $\Delta X + X_{\text{T}} = \frac{1}{\beta}$. X_{T} and ΔX are defined as thresholds for the nearby and far away interferers. If we choose $\Delta X \ll X_{\text{T}}$, the second probability $\Pr\left(X_{\text{near}} \ge X_{\text{T}}\right) \approxeq \Pr\left(X_{\text{near}} \ge \frac{1}{\beta}\right)$. Our approach in (20) is to bound away the effect of faraway interferers and to compute analytical estimates for the effect of nearby interferers, which are basically the cause of packet loss. However, in order to do this effectively and obtain close $\Pr(\text{collision})$ estimates, we must choose radius R_{th} large

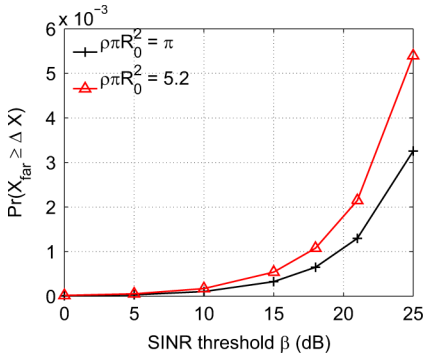

Fig. 11. $\Pr\left(X_{\text{far}} \geq \frac{1}{\beta}\Delta X\right)$ for $R_0 = 100$ m, from (21).

enough such that the faraway interferers are insignificant enough. We choose $R_{\text{th}} = 50R_0$ and $\Delta X_{\text{dB}} = -\beta_{\text{dB}} - 30$ dB, which ensures that $\Pr(X_{\text{far}} \geq \Delta X) < 0.02\Pr(X_{\text{near}} \geq X_{\text{T}})$ for all SINR values β in our setting.

We can bound the first term in (20) using the Markov inequality

$$\Pr(X_{\text{far}} \geq \Delta X) \leq \frac{\mathsf{E}[X_{\text{far}}]}{\Delta X}. \tag{21}$$

The expectation $\mathsf{E}[X_{\text{far}}]$ in (21) can be readily evaluated as

$$\begin{aligned}\mathsf{E}[X_{\text{far}}] &\equiv \frac{\rho}{2\pi}\int_{r=R_{\text{th}}}^{\infty}\int_{\phi_1,\phi_2=-\pi}^{\pi} g(\phi_1)g(\phi_2) \\ &\quad \times \frac{R_0^2}{r^2}e^{-\alpha(r-R_0)}r dr\, d\phi_1\, d\phi_2 \\ &= \frac{(\Delta\phi)^2}{2\pi}\rho R_0^2 e^{\alpha R_0}\int_{r=R_{\text{th}}}^{\infty}\frac{e^{-\alpha r}}{r}dr \end{aligned} \tag{22}$$

where $\Delta\phi$ is the antenna's azimuthal beam angle as defined in (4). Fig. 11 plots $\Pr(X_{\text{far}} \geq \Delta X)$ as a function of β, using (21), for $R_0 = 100$ m assuming flat-top antenna model and different interferer node densities. We will see in Section IV-D that these values are more than an order of magnitude lower than the estimated collision probabilities for these settings.

1) Effect of Nearby Interferers: We now estimate $\Pr(X_{\text{near}} \geq X_{\text{T}})$ in (20), where we first present a simple approach for the flat-top antenna model and then consider general directional antennas.

Each transmitter i inside the circle $C_{R_{\text{th}}}$ causes a random amount of interference $X_i(\phi_1, \phi_2, R)$. The interference random variables $\{X_i\}$ are i.i.d. and are also independent of the number of interferers inside $C_{R_{\text{th}}}$, say N_{th} (N_{th} is Poisson distributed with mean and variance of $\gamma_{\text{th}} = \rho\pi R_{\text{th}}^2$), since conditioned on N_{th}, the location of any given interferer is i.i.d. and uniform inside $C_{R_{\text{th}}}$. Note the two conflicting effects of distance R: The probability of there being an interferer increases with distance R from the receiver $\left(f_{\text{R}}(r) = \frac{2\pi r}{\pi R_{\text{th}}^2}\right)$, but the resulting interference [given by (14)] is drastically low for each interferer located at larger R.

Flat-Top Antenna Model: For a flat-top antenna, the interference threshold X_{T} is exceeded by the nearby interferers under two events, $\mathcal{A}$ and $\mathcal{B}$, defined as follows.

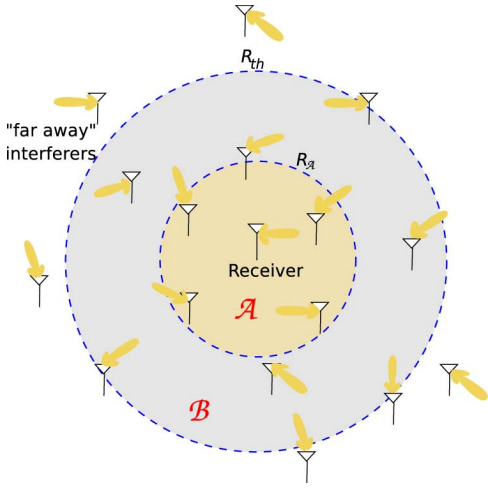

Fig. 12. Flat-top antenna: estimation of $\Pr(X_{\text{near}} \geq X_{\text{T}})$.

$\mathcal{A}$: There is at least one interferer that individually causes interference $\geq X_{\text{T}}$. Note that such an interferer must be within a bounded distance, say $R_{\mathcal{A}}$ of the receiver [$R_{\mathcal{A}} \approx R_i$ defined in (9) for $\Delta X \ll X_{\text{T}}$].

$\mathcal{B}$: The interference beyond $R_{\mathcal{A}}$ sums up to $\geq X_{\text{T}}$.

Events $\mathcal{A}$ and $\mathcal{B}$ are independent events as they correspond to transmitters located in two disjoint spatial regions (illustrated in Fig. 12), the statistics of which are modeled by two independent Poisson processes: $\mathcal{A}$ results from interferers located within range $R_{\mathcal{A}}$ (circle $C_{\mathcal{A}}$) around the receiver, whereas $\mathcal{B}$ depends on the interferers located within the annular region between $R_{\mathcal{A}}$ and R_{th}. Therefore

$$\Pr(X_{\text{near}} \geq X_{\text{T}}) = \Pr(\mathcal{A}) + \Pr(\mathcal{B}) - \Pr(\mathcal{A})\Pr(\mathcal{B}). \tag{23}$$

Consider event $\mathcal{A}$. Let random variable $Y(\phi_1, \phi_2, R_1)$ denote the interference caused by an interferer located within circle $C_{\mathcal{A}}$. Here, $f_{R_1}(r) = \frac{2\pi r}{\pi R_{\mathcal{A}}^2}$ for $r \leq R_{\mathcal{A}}$, and ϕ_1 and ϕ_2 are uniformly distributed over $(-\pi, \pi]$ as earlier. Note that in terms of the general interference random variable $X(\phi_1, \phi_2, R)$, $Y = X(\phi_1, \phi_2, R|R \leq R_{\mathcal{A}})$.

The analysis for $\Pr(\mathcal{A})$ is analogous to that in Section IV-B for the protocol model, where we use (15) with $A = \pi R_{\mathcal{A}}^2$ to obtain the probability of collision $\hat{p}_{\text{c}}$ for an interferer placed at random within $C_{R_{\mathcal{A}}}$. Conditioned on $N_{\mathcal{A}}$, the number of interferers inside $C_{R_{\mathcal{A}}}$, we can estimate the probability that at least one interferer among all interferers in $C_{R_{\mathcal{A}}}$ causes interference $\geq X_{\text{T}}$ as

$$\Pr\left(\max_i Y_i \geq X_{\text{T}} | N_{\mathcal{A}} = k\right) = 1 - (1 - \hat{p}_{\text{c}})^k. \tag{24}$$

$\Pr(\max_i Y_i \geq X_{\text{T}})$ can then be computed by averaging out $N_{\mathcal{A}}$, using the fact that $N_{\mathcal{A}}$ is Poisson distributed with mean $\gamma_{\mathcal{A}} = \rho\pi R_{\mathcal{A}}^2$. We can also substitute $\gamma_{\mathcal{A}}$ in place of k in (24) to obtain a close approximation.

For event $\mathcal{B}$, let $Z(\phi_1, \phi_2, R_2)$ denote the interference random variable corresponding to interferers that lie within the annular region between $R_{\mathcal{A}}$ and R_{th}. We have $f_{R_2}(r) = \frac{2\pi r}{\pi(R_{\text{th}}^2 - R_{\mathcal{A}}^2)}$ for $R_{\mathcal{A}} < r \leq R_{\text{th}}$. Note that $Z = X(\phi_1, \phi_2, R|R_{\mathcal{A}} < R \leq R_{\text{th}})$. We apply the CLT to

estimate $\Pr(\sum_i Z_i \geq X_{\mathrm{T}})$. Conditioned on $N_{\mathcal{B}}$, the number of interferers within the annular region between $R_{\mathcal{A}}$ and R_{th}, we have

$$\Pr\left(\sum_i Z_i \geq X_{\mathrm{T}} | N_{\mathcal{B}} = k\right) = \mathsf{Q}\left(\frac{X_{\mathrm{T}} - k\mathsf{E}[Z]}{\sqrt{k\mathsf{Var}(Z)}}\right) \quad (25)$$

where $\mathsf{Q}(\cdot)$ is the complementary cumulative distribution function for a Normal distribution, given by $\mathsf{Q}(x) = \frac{1}{\sqrt{2\pi}}\int_x^\infty e^{\frac{-x^2}{2}}dx$. The mean $\mathsf{E}[Z]$ is given by

$$\begin{aligned}\mathsf{E}[Z] &= \int_{r=R_{\mathcal{A}}}^{R_{\mathrm{th}}}\iint_{\phi_1,\phi_2=-\pi}^{\pi} g(\phi_1)g(\phi_2)\frac{R_0^2}{r^2}e^{-\alpha(r-R_0)} \\ &\quad \times f_{R_2}(r)\frac{1}{4\pi^2}dr\, d\phi_1\, d\phi_2 \\ &= \frac{(\Delta\phi)^2}{2\pi}\frac{R_0^2}{(R_{\mathrm{th}}^2 - R_{\mathcal{A}}^2)}e^{\alpha R_0}\int_{r=R_{\mathcal{A}}}^{R_{\mathrm{th}}}\frac{e^{-\alpha r}}{r}dr. \end{aligned} \quad (26)$$

$\mathsf{Var}(Z)$ can be evaluated by first computing $\mathsf{E}[Z^2]$ and then using $\mathsf{Var}(Z) = \mathsf{E}[Z^2] - (\mathsf{E}[Z])^2$.

The required probability estimate $\Pr(X_{\mathrm{near}} \geq X_{\mathrm{T}})$ can be computed by averaging out (25) over $N_{\mathcal{B}}$. Given the large expected number of nodes $\gamma_{\mathcal{B}}$ in the annular region between $R_{\mathcal{A}}$ and R_{th}, given by $\gamma_{\mathcal{B}} = \rho\pi(R_{\mathrm{th}}^2 - R_{\mathcal{A}}^2)$ (e.g., for $\rho = 1$ and $R_{\mathrm{th}} = 50R_0$, $\gamma_{\mathcal{B}} = \rho\pi(R_{\mathrm{th}}^2 - R_{\mathcal{A}}^2) \approx 7.8 \cdot 10^3 R_0^2$), we can apply the CLT with mean and variance computed by replacing $N_{\mathcal{B}}$ with $E(N_{\mathcal{B}}) \equiv \gamma_{\mathcal{B}}$, so we obtain

$$\Pr\left(\sum_i Z_i \geq X_{\mathrm{T}}\right) = \mathsf{Q}\left(\frac{X_{\mathrm{T}} - \gamma_{\mathcal{B}}\mathsf{E}[Z]}{\sqrt{\gamma_{\mathcal{B}}\mathsf{Var}(Z)}}\right). \quad (27)$$

In order to obtain an upper bound on $\Pr(\sum_i Z_i \geq X_{\mathrm{T}})$, we apply the Chernoff bound as follows:

$$\Pr\left(\sum_i Z_i \geq X_{\mathrm{T}}\right) \leq \left(\mathsf{E}[e^{s\frac{Z_i}{X_{\mathrm{T}}}}]\right)^{\gamma_{\mathcal{B}}} e^{-s} \quad (28)$$

where the Chernoff bound is derived by minimizing this family of bounds over $s > 0$. Since $\min_{s>0}\left(\mathsf{E}[e^{s\frac{Z_i}{X_{\mathrm{T}}}}]\right)^{\gamma_{\mathcal{B}}} e^{-s}$ has to be obtained via an exhaustive search over a sufficiently large range of values of $s > 0$, the calculation of the Chernoff bound turns out to be computationally expensive.

The flat-top antenna analysis presented above does not apply to general directional antennas because the independence of events $\mathcal{A}$ and $\mathcal{B}$ does not hold. For general directional antennas, even nodes within range $R_{\mathcal{A}}$ of the receiver can cause *nonzero* interference *less than* X_{T} (depending on the relative antenna orientations and gain patterns) due to which event $\mathcal{B}$ can include transmitters within $C_{R_{\mathcal{A}}}$. This is unlike the flat-top antenna case where the antenna gains at both the interferer and the receiver are either 1 or 0, leading to either interference $\geq X_{\mathrm{T}}$ if both nodes are within each other's antenna boresights, or 0 otherwise (which leads to the independence of events $\mathcal{A}$ and $\mathcal{B}$).

General Directional Antennas: We now extend the preceding analysis to general directional antenna patterns, where we derive a CLT-based approximation and obtain an upper bound for $\Pr(X_{\mathrm{near}} \geq X_{\mathrm{T}})$. We use the following expression to estimate $\Pr(X_{\mathrm{near}} \geq X_{\mathrm{T}})$:

$$\begin{aligned}\Pr(X_{\mathrm{near}} \geq X_{\mathrm{T}}) &= \Pr\left(\max_i X_i \geq X_{\mathrm{T}}\right) \\ &\quad + \left(1 - \Pr\left(\max_i X_i \geq X_{\mathrm{T}}\right)\right) \\ &\quad \times \Pr\left(\sum_i X_i \geq X_{\mathrm{T}} | X_i < X_{\mathrm{T}}\ \forall\, i\right). \end{aligned} \quad (29)$$

The first term in the right-hand side (RHS) of (29) captures the probability of cases when the interference from at least one interferer exceeds X_{T} at the intended receiver. The second term captures the cases when there is no single dominant interferer i with $X_i \geq X_{\mathrm{T}}$, but the sum interference from all the interferers exceeds X_{T}. Unlike X_i, the conditional random variable $(X_i | X_i < X_{\mathrm{T}})$ is bounded, its variance is much smaller than that of X_i, and the CLT is better behaved for settings with moderate node densities. Therefore, as we describe in this section, (29) is amenable to obtaining a close approximation via the CLT and an upper bound via the Chernoff bound.

We evaluate the first term $\Pr(\max_i X_i \geq X_{\mathrm{T}})$ of (29) via the protocol model approach (Section IV-B), in a manner analogous to that described for obtaining $\Pr(\mathcal{A})$ in the flat-top antenna model case. We estimate $\Pr(\sum_i X_i \geq X_{\mathrm{T}} | X_i < X_{\mathrm{T}}\ \forall\, i)$ in the second term in the RHS of (29) by applying the CLT to finally obtain

$$\begin{aligned}&\Pr\left(\sum_i X_i \geq X_{\mathrm{T}} | X_i < X_{\mathrm{T}}\ \forall\, i\right) \\ &\quad = \mathsf{Q}\left(\frac{X_{\mathrm{T}} - \gamma_{\mathrm{th}}\mathsf{E}[X_i | X_i < X_{\mathrm{T}}]}{\sqrt{\gamma_{\mathrm{th}}\mathsf{Var}\left(X_i | X_i < X_{\mathrm{T}}\right)}}\right) \end{aligned} \quad (30)$$

where $\mathrm{E}[X_i | X_i < X_{\mathrm{T}}]$ is given by

$$\begin{aligned}&E[X_i | X_i < X_{\mathrm{T}}] \\ &\quad = \int_{r=0}^{R_{\mathrm{th}}}\iint_{\phi_1,\phi_2=-\pi}^{\pi} g(\phi_1)g(\phi_2)\frac{R_0^2}{r^2}e^{-\alpha(r-R_0)} \\ &\qquad \times \mathbf{1}\left(g(\phi_1)g(\phi_2)\frac{R_0^2}{r^2}e^{-\alpha(r-R_0)} < X_{\mathrm{T}}\right) \\ &\qquad \times \frac{f_{\mathrm{R}}(r)}{4\pi^2\Pr\left(X_i < X_{\mathrm{T}}\right)}dr\, d\phi_1\, d\phi_2 \end{aligned} \quad (31)$$

where

$$\begin{aligned}&\Pr\left(X_i < X_{\mathrm{T}}\right) \\ &\quad = \int_{r=0}^{R_{\mathrm{th}}}\iint_{\phi_1,\phi_2=-\pi}^{\pi} \mathbf{1}\left(g(\phi_1)g(\phi_2)\frac{R_0^2}{r^2}e^{-\alpha(r-R_0)} < X_{\mathrm{T}}\right) \\ &\qquad \times f_{\mathrm{R}}(r)\frac{1}{4\pi^2}dr\, d\phi_1\, d\phi_2. \end{aligned} \quad (32)$$

$\mathbf{1}(\cdot)$ above is the indicator function. For calculating $\mathsf{Var}\left(X_i | X_i < X_{\mathrm{T}}\right)$, we first obtain $\mathsf{E}[X_i^2 | X_i < X_{\mathrm{T}}]$ using

a similar approach as shown for $\mathsf{E}[X_i|X_i < X_{\mathrm{T}}]$ and use $\mathsf{Var}\,(X_i|X_i < X_{\mathrm{T}}) = \mathsf{E}[X_i^2|X_i < X_{\mathrm{T}}] - (\mathsf{E}[X_i|X_i < X_{\mathrm{T}}])^2$.

We show in Section IV-D that (29) evaluated using the CLT, when plugged into (20), provides excellent estimates of the interference probability for all scenarios of interest in terms of node densities as well the antenna patterns.

In order to obtain an upper bound on $\Pr\left(X_{\mathrm{near}} \geq X_{\mathrm{T}}\right)$, we first calculate the Chernoff bound for $\Pr\left(\sum_i X_i \geq X_{\mathrm{T}}|X_i < X_{\mathrm{T}}\,\forall\, i\right)$ as

$$\Pr\left(\sum_i X_i \geq X_{\mathrm{T}}|X_i < X_{\mathrm{T}}\,\forall\, i\right) \leq \min_{s>0}\left(\mathsf{E}\left[e^{s\frac{X_i}{X_{\mathrm{T}}}}|X_i < X_{\mathrm{T}}\right]\right)^{\gamma_{\mathrm{th}}} e^{-s}. \quad (33)$$

We then plug this bound in (29) to obtain the desired upper bound. We present the Chernoff bound results for all the examples considered in Section IV-D.

D. Interference Statistics

We now employ our analytical models to estimate collision probabilities for mm-wave mesh networks considering design parameters described in Section III. In particular, we study the dependence of interference statistics on antenna directivities obtained from the link budget analysis for link ranges of 100 and 200 m and spatial deployment density of mesh nodes.

The collision probabilities for the protocol model are computed from (18) and serve as lower bounds for the corresponding collision probabilities from the physical model. We use (20) for the physical model. The first term in (20) is computed from (21) with $R_{\mathrm{th}} = 50R_0$ and $\Delta X_{\mathrm{dB}} = -\beta_{\mathrm{dB}} - 30$ dB. The second term in (20) is estimated via the following methods: 1) using (29) [we also include results from (23) for the flat-top antenna model cases for comparison]; and 2) the use of Monte Carlo simulation, which also serves as a baseline. In addition, by applying the Chernoff bound in place of the CLT for calculating the second term in (20), we obtain an upper bound on $\Pr(\mathrm{collision})$ for all our example settings.

We first consider a set of randomly located/oriented 60-GHz outdoor point-to-point links. The transceiver hardware for such line-of-sight links is commercially available (e.g., [31]). In order to model this setting, we work with moderate spatial node densities that do not necessarily ensure a connected network.

Fig. 13(a) and (b) shows the collision probabilities corresponding to different values of the SINR target β, for link range $R_0 = 100$ m, with ideal flat-top antenna and with a linear array of flat-top elements, respectively, both with a directivity of 24 dBi (required to close the 100-m link; see Section III-A). The beam angle for a flat-top antenna with this directivity is 14.4°, which can be obtained from (2) with the flat-top antenna beam pattern (see the Appendix). The linear array comprises 12 flat-top elements, each of sector width 20°, placed a half-wavelength apart. The azimuthal beam angle for the array [given by (4)] is 8.7°, whereas the azimuthal and vertical half-power beamwidths are 8.5° and 20°, respectively. The spatial node density is such that $\pi\rho R_0^2 = \pi$, and oxygen absorption is 10 dB/km.

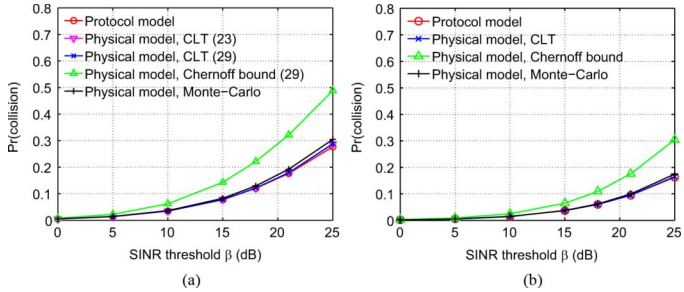

Fig. 13. Collision loss probability for $R_0 = 100$ m, $\pi\rho R_0^2 = \pi$. (a) Flat-top antenna. (b) Linear array.

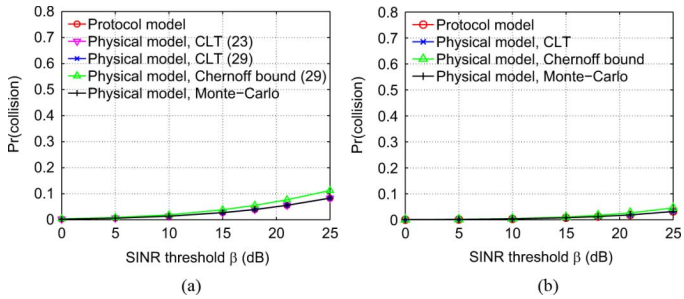

Fig. 14. Collision loss probability for $R_0 = 200$ m, $\pi\rho R_0^2 = \pi$. (a) Flat-top antenna. (b) Linear array.

We observe that for a flat-top antenna, when the desired SINR β increases beyond about 15 dB, the probability of collision approaches 10%, whereas for the linear array, owing to the lower azimuthal beam angle, the probability of collision is relatively low and approaches 10% for $\beta = 21$ dB. To put these results in perspective, note that even a single interferer within the interference range of the receiver would be enough to cause a collision in an omnidirectional setting. We observe that the collision probability estimates under the physical model using the CLT approach and those obtained with Monte Carlo simulations of the nearby interferers are very close to each other and to the corresponding protocol model estimates. Moreover, for the flat-top antenna model, the physical model $\Pr(\mathrm{collision})$ estimates in (20) using (23) to account for the effect of nearby interferers are very close to those obtained via (29). We also observe that the $\Pr(\mathrm{collision})$ upper bounds obtained via the Chernoff bound are loose for this setting, especially at high SINR values.

Fig. 14(a) and (b) shows the interference loss probabilities for ideal flat-top antenna and linear array of flat-top elements for $R_0 = 200$ m. The longer link range of 200 m requires antenna directivity of about 27 dBi, which corresponds to a flat-top antenna of beam angle 10.2° and a linear array of 26 flat-top elements spaced a half-wavelength apart, each with a sector width of 20°. The azimuthal half-power beamwidth of the linear array is about 4°. The other parameters are the same as the preceding case of $R_0 = 100$ m. From the plots, it is clear that for the 200-m link range, the higher antenna directivity reduces the interference loss probability even further relative to that for 100-m links. Also, in this highly directional setting, $\Pr(\mathrm{collision})$ estimates obtained via all the models are very close to each other, and $\Pr(\mathrm{collision})$ upper bounds obtained

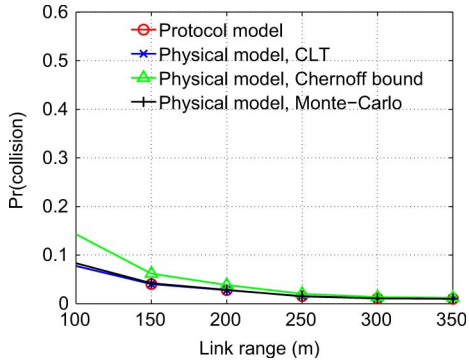

Fig. 15. Collision loss probability for the flat-top antenna model with increasing link range R_0 and $\pi\rho R_0^2 = \pi$.

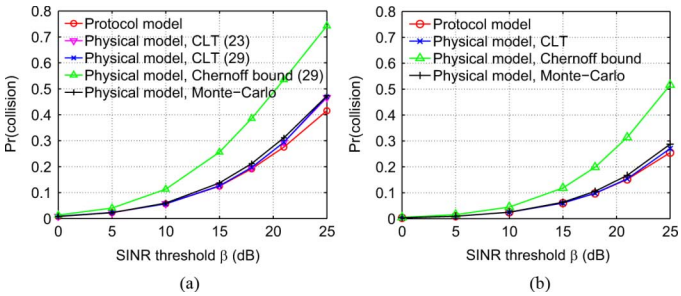

Fig. 16. Collision loss probability for $R_0 = 100$ m, $\pi\rho R_0^2 = 5.2$. (a) Flat-top antenna. (b) Linear array.

via the Chernoff bound are relatively tight. Fig. 15 illustrates the reduction in the collision probability with increasing link range, where we plot $\Pr(\text{collision})$ for flat-top antennas with different beam angles corresponding to link ranges varying from 100 to 350 m, with the other link budget parameters same as in Section III-A.

The key observation from the above results is that the packet loss due to interference is expected to be very low for mm-wave mesh networks with the node density and SINR parameters of interest to us. Furthermore, the probability of collision under the physical model does not appreciably differ from the protocol model, particularly for collision probabilities of 10% or less, implying that the protocol model estimates work well in this desired regime of operation.

We now consider higher mesh node deployment densities that guarantee a connected network with a high probability. Note that the capability to sense and beam-steer toward a neighbor in any azimuthal direction implies that the connectivity versus spatial node density results for omnidirectional networks apply in this setting. In order to calculate the required node densities, we employ the analytical model and connectivity results presented in [32]. Ignoring border effects (which is reasonable for large networks), we obtain that for $R_0 = 100$ m, $\pi\rho R_0^2 = 5.2$ ensures a connected network with a high probability of 0.99, whereas for $R_0 = 200$ m, the required value is $\pi\rho R_0^2 = 4.4$. Note that ρ is the spatial density of transmit nodes, which is assumed to be less than half of that for all nodes. Fig. 16(a) and (b) shows the collision probabilities for the ideal flat-top antenna and for the linear array, respectively, for link range $R_0 = 100$ m. The $\Pr(\text{collision})$ estimates for the physical model are greater

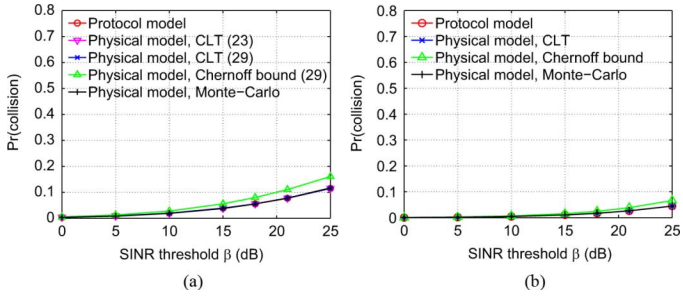

Fig. 17. Collision loss probability for $R_0 = 200$ m, $\pi\rho R_0^2 = 4.4$. (a) Flat-top antenna. (b) Linear array.

than those obtained under the protocol model for higher values of the desired SINR (e.g., ≥ 18 dB). The reason for this difference is that the increasing effect of the sum interference (with higher node densities) that leads to more collisions for higher SINR is not captured by the protocol model. We also observe that the $\Pr(\text{collision})$ upper bounds obtained via the Chernoff bound are very loose for this case, especially for higher SINR targets. Fig. 17(a) and (b) plot the interference loss probabilities for ideal flat-top antenna and linear array of flat-top elements for $R_0 = 200$ m. Although the probability of collision in each case is comparatively higher than the corresponding setting with a lower node density [Fig. 14(a) and (b)], the previous observation of substantially low interference loss probabilities relative to omnidirectional communication settings still applies.

E. Pseudowired Abstraction

The preceding interference analysis results show that for mm-wave mesh networks with moderate to high node densities, even with uncoordinated transmissions, the collision probabilities are very small for the parameters corresponding to the reference link budget described in Section III-A. This observation points to a very different paradigm from that normally encountered in wireless networks, where interference substantially limits spatial reuse. Furthermore, the probability of collision under the protocol model is very close to that with the physical model in the desired regime of operation with lower collision probabilities (e.g., $\leq 10\%$) and for the purpose of interference analysis, details of antenna beam-patterns can be abstracted away using the notion of equivalent flat-top beam angles. This suggests that MAC protocols for mm-wave mesh networks need not be focused on minimizing packet loss from interference. Instead, the focus of MAC design should be on overcoming the challenging problem of scheduling under deafness constraints. We conclude that the MAC designer can use the following *pseudowired abstraction* as a starting point.

1) *No interference*. Transmissions between two distinct pairs of nodes are unlikely to interfere with each other and interference can be largely ignored in MAC design.
2) *Half-duplex constraint*. Each node can either transmit or receive at any given time, but not both.

V. MAC Simulations

The results in Section IV indicate that we can essentially ignore interference and the details of antenna patterns in the *design* of medium access control for mm-wave mesh networks, al-

though their effect on *performance* must be quantified. This is a distinct advantage over directional networking at lower carrier frequencies, where it is difficult to achieve such high link directivities. On the other hand, the high directivity of mm-wave links also implies that mm-wave mesh nodes are essentially deaf to their neighbors, which poses a challenge in coordinating transmissions.

To verify the pseudowired abstraction and highlight its effects on network performance, we simulate a naive directional slotted Aloha protocol. Prior studies on slotted Aloha with directional communication include [20], [33], and [34], but unlike these papers, our goal is to examine the relative effects of interference and deafness on performance. We note that far better performance can be obtained using more sophisticated MAC designs. Our own related publication [8] proposes one such MAC protocol.

Our approach to compare the packet loss because of interference and lack of transmit–receive coordination for slotted Aloha is the following. We obtain the number of packets that are not decoded correctly by the intended receivers because of external interference (which depends on the corresponding SINR at each intended receiver). We define transmit–receive coordination loss as the packet loss either because the intended receiver was beamformed in a direction other than that toward the transmit node under consideration (leading to poor antenna gain in the direction of the transmit node) or because the intended receiver was also transmitting a packet during the slot. We compare the ratio of these losses with respect to the total number of packet transmissions.

1) Simulation Setup: We consider random network topologies with 25 or 50 nodes spread over a 500×500 m^2 flat terrain. Every node initiates one constant bit rate (CBR) flow to each of its neighbors, at a large enough data rate (1 Gb/s) to saturate the link. Under the directional slotted Aloha protocol, whenever a node has a new packet to transmit, it beamforms toward the direction of the intended receiver and transmits the packet in the next slot. If the node does not receive an ACK, it attempts to retransmit the packet with a probability p_{retx} over the next slots. A node returns to the unbacklogged state after every successful packet transmission.

We consider a sectorized antenna design with each sector covered by an array of high-gain antenna elements. For concreteness, we consider endfire patch antenna elements that can be realized as patterns of metal on a circuit board [35]. Each element has azimuthal and vertical half-power beamwidths of about 33° and 45°, respectively, which leads to a directivity of 14 dBi. The element gain patterns are shown in Fig. 18. In order to obtain the desired array directivity of 24 dBi, we need a linear array of 25 elements spaced a half-wavelength apart. The azimuthal half-power beamwidth of the resulting array is about 4°.

We use the QualNet network simulator [36] for our simulations. We have modified the QualNet PHY and Antenna modules to model propagation in the mm-wave band and our link budget design.

2) Results: Fig. 19(a) and (b) shows the interference loss and the transmit–receive coordination failure loss for 25 and 50 node random topologies as a function of slotted Aloha retransmit probability p_{retx}. The loss figures are relative to the total number of packet transmissions. Fig. 19(c) shows the corresponding aggregate network throughput. Comparing Fig. 19(a) and (b), we observe that the interference loss is about an order of magnitude lower than the coordination loss in this setting, which indicates that transmit–receive coordination is a significantly bigger challenge than interference. As the retransmission probability increases, nodes become more aggressive in attempting transmissions after reception failures, which leads to higher coordination loss, as illustrated in Fig. 19(b). This results in reduced aggregate throughput seen in Fig. 19(c). An interesting observation from Fig. 19(b) is that the coordination loss values are close for the 25- and 50-node topologies. This can be explained as follows. Coordination loss occurs either because the intended receiver is transmitting or it is beamformed toward a different direction for reception. Under a saturated traffic model, each node always has backlogged packet queues, so the probability that a node chooses to transmit in a given slot is independent of spatial density of nodes. In case the intended receiver chooses not to transmit, the probability that it beamforms toward a different direction depends on the probability that at least one of the other neighbors (in addition to the tagged transmit node) of the intended receiver chooses to transmit to that node. The increasing node density has two opposing effects on this probability: The probability that at least one of the other neighbors chooses to transmit increases with node density, but the probability that the transmission is intended for the tagged receiver node decreases with increasing node density (i.e., more neighbors for each node). This leads to similar coordination losses for the 25- and 50-node random topologies.

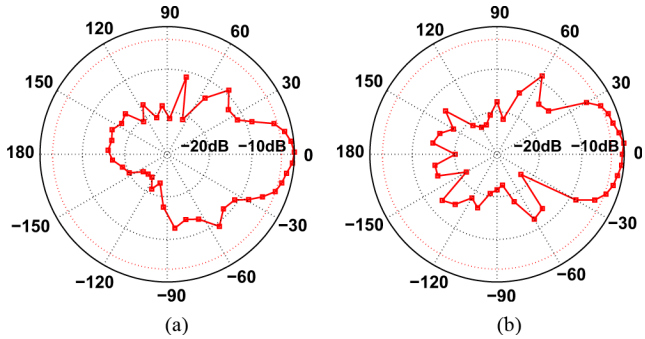

Fig. 18. Patch antenna gain pattern. (a) H-plane. (b) E-plane.

Note that the following two points are important while interpreting the directional slotted Aloha results in light of the interference analysis presented earlier. 1) Our interference analysis finds the probability of packet loss due to interference, conditioned on the assumption that the tagged transmitter and the receiver are beamformed toward each other. We do not consider transmit–receive coordination loss in our analysis. 2) The interference loss for our simulation setting is expected to be lower relative to that obtained for the flat-top antenna and linear arrays in Section IV-D because of the narrower azimuthal half-power beamwidth of the patch antenna array (4° versus 14.4° and 8.5°: Given the relatively smaller vertical beamwidths of the flat-top antenna and also the flat-top elements to construct the linear array, the required azimuthal half-power beamwidths to obtain the same directivity are larger). In other words, our analytical

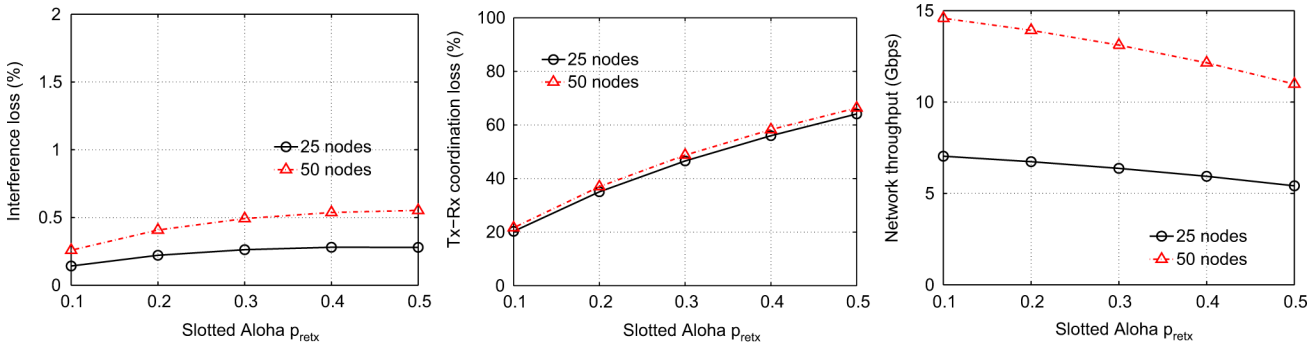

Fig. 19. Simulation results for directional slotted Aloha protocol. (a) Interference loss. (b) Transmit–receive coordination loss. (c) Aggregate network throughput.

results on the interference loss are more conservative than the simulations.

The low interference loss results for the slotted Aloha example indicate that the pseudowired abstraction for mm-wave mesh network links can indeed serve as an appropriate first-order approximation for MAC design in highly directional mm-wave mesh networks. Therefore, the challenge for the network designer is to schedule transmissions in the face of deafness resulting from the highly directional links while exploiting the reduced interference among simultaneously active mm-wave links.

VI. Conclusion and Future Work

We have investigated the impact of the unique physical characteristics of mm-wave links on the statistics of spatial interference and consequently MAC design for outdoor mm-wave mesh networks. Our interference analysis framework enables a quantitative evaluation of collision loss probability for a mm-wave mesh network with uncoordinated transmissions, as a function of the antenna patterns and spatial density of simultaneously transmitting nodes. For the directivities typical of mm-wave nodes with compact form factors, the low collision loss probabilities indicate that the pseudowired model is indeed appropriate, which motivates a radically different approach to MAC design relative to the CSMA-based WiFi mesh networks operating in the low frequency bands. Rather than focusing on proactive interference management as in conventional MAC design, we must now devise scheduling mechanisms that address deafness.

We note that preliminary results [8] for Memory-guided Directional MAC (MDMAC), a MAC protocol designed according to these guidelines, are promising. However, there are a number of important topics for future research in the design of mm-wave mesh networks. It is important to devise automated network discovery and topology update mechanisms, closely coupled with efficient mechanisms for transmit and receive beamforming. Another key issue is that of packet-level time synchronization. For example, the MDMAC protocol in [8] uses learning and predictability to combat deafness, but is predicated on network-wide time slotting. Lightweight mechanisms need to be developed for acquiring and maintaining such time slotting in highly directional networks. We also need more detailed propagation models: While rooftop-to-rooftop links may be well approximated as idealized line-of-sight links, links in a lamppost-based network may exhibit severe fading even with the sparse multipath corresponding to a highly directional link [37]. This has an impact both on physical-layer design (e.g., providing antenna diversity) and network architecture (e.g., providing route diversity). Finally, design for indoor mm-wave mesh networks must address additional challenges of blockage and coexistence.

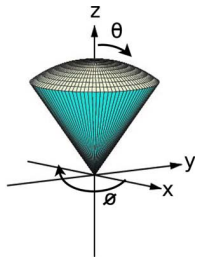

Fig. 20. Flat-top antenna pattern in polar coordinates (θ, ϕ) around the antenna beam axis.

Appendix

Antenna Directivity Computations: We use (2) in order to calculate the exact antenna directivity from the antenna pattern. We first need to compute the beam solid angle $\Omega = \int_{\theta=0}^{\pi} \int_{\phi=-\pi}^{\pi} G_{\mathrm{n}}(\theta,\phi) \sin\theta \; d\theta \; d\phi$ of the antenna, where $G_{\mathrm{n}}(\theta,\phi)$ is the normalized power pattern.

Flat-Top Antenna: Looking at the 3-D pattern for a flat-top antenna with sector width w, in polar coordinates (θ,ϕ) around the antenna beam axis (see Fig. 20), we have

$$G_{\mathrm{n}}(\theta,\phi) = \begin{cases} 1, & -\pi \le \phi \le \pi,\ 0 \le \theta \le \frac{w}{2} \\ 0, & \text{otherwise.} \end{cases} \tag{34}$$

Therefore

$$\begin{aligned} \Omega &= \int_{\theta=0}^{\pi} \int_{\phi=-\pi}^{\pi} G_{\mathrm{n}}(\theta,\phi) \sin\theta \; d\theta \; d\phi \\ &= \int_{\theta=0}^{\frac{w}{2}} \int_{\phi=-\pi}^{\pi} \sin\theta \; d\theta \; d\phi \\ &= 2\pi \left(1 - \cos\left(\frac{w}{2}\right)\right). \end{aligned} \tag{35}$$

Therefore, directivity D of the flat-top antenna is given by

$$D = \frac{4\pi}{2\pi\left(1-\cos\left(\frac{w}{2}\right)\right)} = \frac{2}{1-\cos\left(\frac{w}{2}\right)}. \tag{36}$$

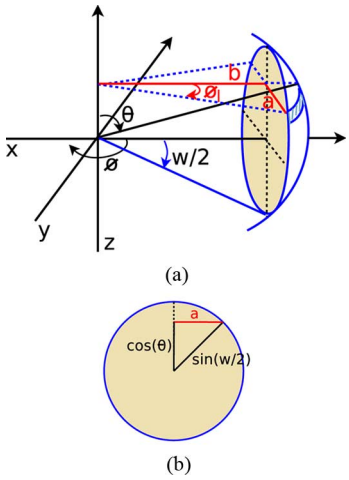

Fig. 21. Linear array of flat-top elements: directivity calculation. (a) Geometry of the 3-D antenna pattern. (b) Calculation of a.

For $D = 24$ dBi, we obtain $w = 14.4°$, which is the required flat-top antenna sector width for our 100-m mm-wave mesh link example.

Linear Array of Flat-Top Antenna Elements: For a simpler approach to calculation of the beam solid angle in case of a uniform linear array of flat-top elements spaced $\lambda/2$ apart, we reorient the antenna pattern with the beam axis along the x-axis (i.e., the antenna elements in the array are placed along the y-axis), as shown in Fig. 21(a). The normalized 3-D antenna pattern for a linear array of N flat-top elements, each with a beamwidth w, in this coordinate system is given by

$$G_{\rm n}(\theta,\phi) = \begin{cases} \frac{1}{N^2}\frac{\sin^2\left(\frac{N}{2}\pi\cos\theta\right)}{\sin^2\left(\frac{1}{2}\pi\cos\theta\right)}, & -\phi_l(\theta) \le \phi \le \phi_l(\theta), \\ & \frac{\pi}{2} - \frac{w}{2} \le \theta \le \frac{\pi}{2} + \frac{w}{2} \\ 0, & \text{otherwise.} \end{cases} \tag{37}$$

We now derive $\phi_l(\theta)$ as a function of the polar angle θ. Consider the circle formed by the intersection of the 3-D flat-top antenna pattern with the surface of the (normalized) unit sphere centered at the antenna (Fig. 21). From Fig. 21(a), for a given θ, the limits of integration for ϕ are given by $\pm\phi_l$ where $\phi_l = \tan^{-1}\left(\frac{a}{b}\right)$ and $|\phi_l| \le \frac{\pi}{2}$. We have $b = \cos\frac{w}{2}$, and from Fig. 21(b), $a(\theta) = \left(\sin^2\left(\frac{w}{2}\right) - \cos^2\theta\right)^{\frac{1}{2}}$. Therefore, $\phi_l(\theta) = \tan^{-1}\left(\frac{\left(\sin^2\left(\frac{w}{2}\right)-\cos^2\theta\right)^{\frac{1}{2}}}{\cos\left(\frac{w}{2}\right)}\right)$. We now compute Ω for a linear array of flat-top elements as follows:

$$\begin{aligned} \Omega &= \int_{\theta=0}^{\pi}\int_{\phi=-\pi}^{\pi} G_{\rm n}(\theta,\phi)\sin\theta\, d\theta\, d\phi \\ &= \int_{\theta=\frac{\pi}{2}-\frac{w}{2}}^{\frac{\pi}{2}+\frac{w}{2}}\int_{\phi=-\phi_l(\theta)}^{\phi_l(\theta)} \\ &\quad \times \frac{1}{N^2}\frac{\sin^2\left(\frac{N}{2}\pi\cos\theta\right)}{\sin^2\left(\frac{1}{2}\pi\cos\theta\right)}\sin\theta\, d\theta\, d\phi. \end{aligned} \tag{38}$$

Consider an example antenna array design problem: How many flat-top antenna elements, each of sector-width 20°, spaced a half-wavelength $(\lambda/2)$ apart to form a uniform linear array, are needed to attain directivity $D = 24$ dBi? Using the calculations outlined above, we find that a linear array of 12 flat-top elements provides the required directivity. We use this linear array for the 100-m mm-wave link examples in the paper. Note that we can also derive the directivity of a flat-top antenna element in a similar fashion, with the antenna beam axis along the x-axis [i.e., $G_{\rm n}(\theta,\phi) = 1$ for the same (θ,ϕ) limits as in (37)].

REFERENCES

[1] "Wireless Gigabit Alliance," Wireless Gigabit Alliance, Beaverton, OR [Online]. Available: http://wirelessgigabitalliance.org/

[2] "IEEE 802.15 WPAN Task Group 3c (TG3c) Millimeter Wave Alternative PHY," IEEE, Piscataway, NJ [Online]. Available: http://www.ieee802.org/15/pub/TG3c.html

[3] "ECMA International," ECMA, Geneva, Switzerland [Online]. Available: http://www.ecma-international.org/

[4] "Very High Throughput in 60 GHz," IEEE 802.11 TGad, Piscataway, NJ, 2010 [Online]. Available: http://www.ieee802.org/11/Reports/tgad_update.htm

[5] "WirelessHD," WirelessHD [Online]. Available: http://wirelesshd.org/

[6] S. Alalusi and R. Brodersen, "A 60 GHz phased array in CMOS," in *Proc. IEEE CICC*, Sep. 2006, pp. 393–396.

[7] D. Liu and R. Sirdeshmukh, "A patch array antenna for 60 GHz package applications," in *Proc. IEEE AP-S Symp.*, Jul. 2008, pp. 1–4.

[8] S. Singh, R. Mudumbai, and U. Madhow, "Distributed coordination with deaf neighbors: Efficient medium access for 60 GHz mesh networks," in *Proc. IEEE INFOCOM*, Mar. 2010, pp. 1–9.

[9] P. Gupta and P. R. Kumar, "The capacity of wireless networks," *IEEE Trans. Inf. Theory*, vol. 46, no. 2, pp. 388–404, Mar. 2000.

[10] R. Mudumbai, S. Singh, and U. Madhow, "Medium access control for 60 GHz outdoor mesh networks with highly directional links," in *Proc. IEEE INFOCOM*, Apr. 2009, pp. 2871–2875.

[11] P. F. M. Smulders, "Exploiting the 60 GHz band for local wireless multimedia access: Prospects and future directions," *IEEE Commun. Mag.*, vol. 40, no. 1, pp. 140–147, Jan. 2002.

[12] S. Singh, F. Ziliotto, U. Madhow, E. Belding, and M. Rodwell, "Blockage and directivity in 60 GHz wireless personal area networks: From cross-layer model to multihop MAC design," *IEEE J. Sel. Areas Commun.*, vol. 27, no. 8, pp. 1400–1413, Oct. 2009.

[13] "Millimeter Wave Communication Systems Research @ UCSB," Wireless Communication and Sensornets Laboratory, ECE Department, University of California, Santa Barbara, CA [Online]. Available: www.ece.ucsb.edu/wcsl/mmwcsresearch/doku.php

[14] R. R. Choudhury, X. Yang, R. Ramanathan, and N. H. Vaidya, "On designing MAC protocols for wireless networks using directional antennas," *IEEE Trans. Mobile Comput.*, vol. 5, no. 5, pp. 477–491, May 2006.

[15] R. Ramanathan, J. Redi, C. Santivanez, D. Wiggins, and S. Polit, "Ad hoc networking with directional antennas: A complete system solution," *IEEE J. Sel. Areas Commun.*, vol. 23, no. 3, pp. 496–506, Mar. 2005.

[16] T. Korakis, G. Jakllari, and L. Tassiulas, "CDR-MAC: A protocol for full exploitation of directional antennas in ad hoc wireless networks," *IEEE Trans. Mobile Comput.*, vol. 7, no. 2, pp. 145–155, Feb. 2008.

[17] A. Nasipuri, S. Ye, J. You, and R. Hiromoto, "A MAC protocol for mobile ad hoc networks using directional antennas," in *Proc. IEEE WCNC*, 2000, vol. 3, pp. 1214–1219.

[18] M. Takai, J. Martin, R. Bagrodia, and A. Ren, "Directional virtual carrier sensing for directional antennas in mobile ad hoc networks," in *Proc. ACM MobiHoc*, New York, 2002, pp. 183–193.

[19] R. Choudhury and N. Vaidya, "Deafness: A MAC problem in ad hoc networks when using directional antennas," in *Proc. IEEE ICNP*, 2004, pp. 283–292.

[20] H. Singh and S. Singh, "Smart-ALOHA for multi-hop wireless networks," *Mobile Netw. Appl.*, vol. 10, no. 5, pp. 651–662, 2005.

[21] G. Jakllari, W. Luo, and S. V. Krishnamurthy, "An integrated neighbor discovery and MAC protocol for ad hoc networks using directional antennas," in *Proc. IEEE WoWMoM*, Washington, DC, 2005, pp. 11–21.

[22] S. Kulkarni and C. Rosenberg, "DBSMA: A MAC protocol for multi-hop ad-hoc networks with directional antennas," in *Proc. IEEE PIMRC*, Sep. 2005, vol. 2, pp. 1371–1377.

[23] L. Tong, V. Naware, and P. Venkitasubramaniam, "Signal processing in random access," *IEEE Signal Process. Mag.*, vol. 21, no. 5, pp. 29–39, Sep. 2004.

[24] M. Pursley, "Performance evaluation for phase-coded spread-spectrum multiple-access communication—Part I: System analysis," *IEEE Trans. Commun.*, vol. 25, no. 8, pp. 795–799, Aug. 1977.

[25] G. Efthymoglou, V. Aalo, and H. Helmken, "Performance analysis of coherent DS-CDMA systems in a Nakagami fading channel with arbitrary parameters," *IEEE Trans. Veh. Technol.*, vol. 46, no. 2, pp. 289–297, May 1997.
[26] M. Sunay and P. McLane, "Calculating error probabilities for DS-CDMA systems: When not to use the Gaussian approximation," in *Proc. IEEE GLOBECOM*, 1996, vol. 3, pp. 1744–1749.
[27] A. Iyer, C. Rosenberg, and A. Karnik, "What is the right model for wireless channel interference?," *IEEE Trans. Wireless Commun.*, vol. 8, no. 5, pp. 2662–2671, May 2009.
[28] S. Weber, J. G. Andrews, and N. Jindal, "An overview of the transmission capacity of wireless networks," *CoRR*, 2010, Abs/0809.0016.
[29] F. Giannetti, M. Luise, and R. Reggiannini, "Mobile and personal communications in the 60 GHz band: A survey," *Wireless Pers. Commun.*, vol. 10, no. 2, pp. 207–243, Jul. 1999.
[30] R. Mudumbai and U. Madhow, "Information theoretic bounds for sensor network localization," in *Proc. IEEE ISIT*, Jul. 2008, pp. 1602–1606.
[31] "Proxim Wireless GigaLink series," Proxim Wireless, Milpitas, CA [Online]. Available: http://www.proxim.com/products/gigalink/
[32] C. Bettstetter, "On the connectivity of ad hoc networks," *Comput. J.*, vol. 47, no. 4, pp. 432–447, 2004.
[33] J. Zander, "Slotted ALOHA multihop packet radio networks with directional antennas," *Electron. Lett.*, vol. 26, no. 25, pp. 2098–2100, Dec. 1990.
[34] J. Ward and R. T. Compton, "Improving the performance of a slotted Aloha packet radio network with an adaptive array," *IEEE Trans. Commun.*, vol. 40, no. 2, pp. 292–300, Feb. 1992.
[35] M. Seo, B. Ananthasubramaniam, M. Rodwell, and U. Madhow, "Millimeterwave imaging sensor nets: A scalable 60-GHz wireless sensor network," in *Proc. IEEE MTT-S IMS*, Jun. 2007, pp. 563–566.
[36] "QualNet, V4.1," Scalable Network Technologies, Los Angeles, CA [Online]. Available: http://www.scalable-networks.com
[37] H. Zhang, S. Venkateswaran, and U. Madhow, "Channel modeling and MIMO capacity for outdoor millimeter wave links," in *Proc. IEEE WCNC*, Sydney, Australia, Apr. 2010, pp. 1–6.

Sumit Singh (M'10) received the Bachelor's degree in electrical engineering from the Indian Institute of Technology, Bombay, India, in 2002, and the Master's and Ph.D. degrees in electrical and computer engineering from the University of California (UC), Santa Barbara, in 2006 and 2009, respectively.

He was a Software Engineer with the Network Systems Division, Samsung Electronics, Bangalore, India, from 2002 to 2004. He was a Post-Doctoral Researcher with UC Santa Barbara from 2009 to 2010, and is currently a Wireless Architect with the Moseley Wireless Solutions Group, Santa Barbara, CA. His research interests lie in wireless networking, particularly medium access control, resource allocation, and quality of service in wireless networks.

Raghuraman Mudumbai (S'04–M'09) received the B.Tech. degree in electrical engineering from the Indian Institute of Technology, Madras, India, in 1998, the M.S.E.E. degree from the Polytechnic University, Brooklyn, NY, in 2000, and the Ph.D. degree in electrical and computer engineering from the University of California, Santa Barbara, in 2007.

He joined the Electrical and Computer Engineering Department, The University of Iowa, Iowa City, in August 2009, where he is currently an Assistant Professor.

Upamanyu Madhow (S'86–M'90–SM'96–F'05) received the Bachelor's degree from the Indian Institute of Technology, Kanpur, India, in 1985, and the Ph.D. degree from the University of Illinois at Urbana–Champaign in 1990, both in electrical engineering.

He was a Research Scientist with Bell Communications Research, Morristown, NJ, and a faculty member with the University of Illinois at Urbana–Champaign. He is currently a Professor of electrical and computer engineering with the University of California, Santa Barbara. He is the author of the textbook *Fundamentals of Digital Communication* (Cambridge Univ. Press, 2008). His research interests are in communication systems and networking, with current emphasis on wireless communication, sensor networks, and multimedia security.

Dr. Madhow has served as an Associate Editor for the IEEE TRANSACTIONS ON COMMUNICATIONS, the IEEE TRANSACTIONS ON INFORMATION THEORY, and the IEEE TRANSACTIONS ON INFORMATION FORENSICS AND SECURITY. He is a recipient of the NSF CAREER award.